90-4

$IN-$

# NASA

# MEMORANDUM

HYDRODYNAMIC IMPACT-LOAD ALLEVIATION

WITH A PENETRATING HYDRO-SKI

By Philip M. Edge, Jr.

Langley Research Center
Langley Field, Va.

# NATIONAL AERONAUTICS AND SPACE ADMINISTRATION
## WASHINGTON
February 1959

NATIONAL AERONAUTICS AND SPACE ADMINISTRATION

MEMORANDUM 1-9-59L

HYDRODYNAMIC IMPACT-LOAD ALLEVIATION

WITH A PENETRATING HYDRO-SKI

By Philip M. Edge, Jr.

## SUMMARY

A penetrating hydro-ski was mounted below a model tested previously in the study reported in NACA Technical Note 4401, and a series of impacts were made in the Langley impact basin to determine load alleviation with this type of hydro-ski. The hydro-ski was designed to penetrate through seaway irregularities with a minimum of drag and with small impact loads. The penetrating hydro-ski was small (beam-loading coefficient of 111) and of a streamline shape with the bottom designed for flush retraction into the main model.

A series of impacts at fixed trim angles of $8^\circ$, $16^\circ$, and $30^\circ$ were made in smooth water and at a fixed trim angle of $8^\circ$ in rough water. The loads and motions of the model were recorded, and photographic observations of the flow and cavities generated in the water by the penetrating hydro-ski were made.

The data are presented and the maximum impact loads and maximum drafts of the model with the penetrating hydro-ski are compared with those of the model obtained without the penetrating hydro-ski. Maximum load reductions of 30 to 70 percent in smooth water and of 50 to 80 percent in rough water are indicated. Cavity and flow generation by the penetrating hydro-ski are discussed, and it is indicated that the penetrating hydro-ski moved smoothly through the water and generated deep cavities which are shown by stereophotographs.

## INTRODUCTION

In the design of high-speed, high-density water-based aircraft a basic hydrodynamic problem consists of obtaining a configuration which will provide adequate lift at low speeds during taxiing, taking off, or landing and, in turn, have low impact loads. In general, configurations with desirable lift characteristics for achieving a minimum hump speed are the very configurations for which severe impact loads are experienced at high speeds in rough water. Means of alleviating these loads have

been considered, and some reduction has been obtained with hydro-ski applications and with improved hull and hydro-ski configurations. The fundamentals of impact loads as related to body configuration have been the subject of extensive experimental research at the Langley impact basin (refs. 1 to 11). Included in these studies have been models of extremely high beam loading (beam loading coefficients as high as 540 in ref. 11).

One solution to this problem of load reduction is the use of a penetrating hydro-ski mounted below a hull or mounted as a sub-ski below the main hydro-ski of the aircraft. The penetrating hydro-ski is a small hydro-ski of high beam loading and is designed for complete immersion in the water at moderate speeds. The function of the penetrating hydro-ski is to penetrate through seaway irregularities (wave crests and so forth) with a minimum of drag load and with designed impact loads limited by small size, by clean shape, and by the location below the aircraft. In effect, the penetrating hydro-ski, because of its small size, applies a temporary cut-off of the impact load developed. The distance the penetrating hydro-ski is mounted below the main body determines the stroke through which this cut-off acts or the height of wave in which it can operate. Furthermore, the penetrating hydro-ski is intended to alleviate the load applied to the main body by generating a cavity in the surface of the water normally contacted by the main body. The small size and the shape of this type of hydro-ski permits adjustable mounting and complete retraction into the main body to form a conventional configuration for optimum low-speed operation.

In order to obtain experimental data on the load-alleviation possibilities of a penetrating hydro-ski, a series of impacts were made in the Langley impact basin with a small hydro-ski (beam-loading coefficient of 111) mounted below a main model (beam-loading coefficient of 3.6) whose impact-load characteristics had been studied previously (ref. 10). Impacts at fixed trim angles were made over a range of trim and flight-path angles in smooth water. Impacts were made in rough water with short, choppy waves having crest-to-crest lengths less than two model lengths. Loads and motions of the main model were measured, along with wave heights and lengths. Observations of the cavity and flow generated by the hydro-ski were made from motion pictures and from stereophotographs.

The data obtained with the model equipped with the penetrating hydro-ski are presented and the maximum loads and maximum drafts are compared with those obtained without the penetrating hydro-ski. The load-alleviating effects of the hydro-ski are indicated for smooth and rough water. Stereophotographs are presented to illustrate the character and magnitude of the cavity generated by the hydro-ski.

SYMBOLS

| | |
|---|---|
| $b$ | model beam, ft |
| $C_d$ | draft coefficient, $\dfrac{z}{b}$ |
| $C_L$ | impact-lift coefficient, $\dfrac{n_i W}{\frac{1}{2}\rho V_o^2 b^2} = \dfrac{F_v}{\frac{1}{2}\rho V_o^2 b^2}$ |
| $C_\Delta$ | beam-loading coefficient, $\dfrac{W}{\rho g b^3}$ |
| $F_v$ | vertical component of hydrodynamic force, lb |
| $g$ | acceleration due to gravity, 32.2 ft/sec$^2$ |
| $h$ | wave height measured from trough to crest, ft |
| $l$ | wave length measured from trough to trough, ft |
| $n_i$ | impact-load factor normal to undisturbed water surface, $\dfrac{F_v}{W}$ |
| $t$ | time after first contact, sec |
| $V$ | resultant velocity of model, ft/sec |
| $W$ | dropping weight, lb |
| $\dot{x}$ | velocity of model parallel to undisturbed water surface, ft/sec |
| $z$ | draft of model normal to undisturbed water surface, ft |
| $\dot{z}$ | velocity of model normal to undisturbed water surface, ft/sec |
| $\gamma$ | flight-path angle relative to undisturbed water surface, deg |
| $\theta$ | a measure of wave slope, $\tan^{-1}\dfrac{2h}{l}$, deg |
| $\rho$ | mass density of water, 1.938 slugs/cu ft |
| $\tau$ | trim angle, deg |

4

Subscripts:

max       maximum

o         instant of initial contact with water surface


APPARATUS


Tests were made in the Langley impact basin with the equipment
described in reference 12. This equipment consists of a catapult, a
testing carriage to which the model is attached, instrumentation for
measuring loads and motions of the model, and an arresting gear. The
model is attached to the carriage at all times by a boom mounted on a
parallel linkage which permits the model to move freely in the vertical
direction. The waves used in the rough-water tests were generated by
the wavemaker described in reference 13.


Model and Hydro-Ski

Detail lines of the model and the penetrating hydro-ski are shown
in figure 1. The plan form of the model was V-shape at each end with a
5-foot section of constant beam (22 inches) in the center. The angle
of the V plan form at the stern was 60° and at the bow, 30°. The
transverse shape, as shown in figure 1, was circular at the keel and
had a straight dead rise of about 35° midway, with chines flaring to
horizontal. The penetrating hydro-ski was mounted below the center of
the center section of the model at a distance of 19.2 inches. The plan
form of the hydro-ski was formed by two circular arcs which had a ratio
of length to beam equal to 8 (length = 56 in, beam = 7 in.). The pro-
file of the hydro-ski was formed by a circular-arc at the top and had
a straight-keel bottom. The straight-keel bottom and the circular-arc
transverse shape of the hydro-ski were made the same as for the model
so as to simulate a fully retractable ski. The steel strut upon which
the penetrating hydro-ski was mounted was also of circular-arc cross
section 4 inches long by 3/8 inch wide. The bow of the hydro-ski was
braced by two rods of 1/4-inch diameter attached to the chine of the
main model. Both the model and the hydro-ski were constructed of wood
covered with fiber glass.

Figure 2 shows the model with the penetrating hydro-ski mounted on
the carriage boom. This mounting held the model at a fixed trim angle
throughout the impacts.

## Instrumentation

The instrumentation consisted of a multichannel oscillograph, pick-ups for measuring loads and motions, an NACA optical wave-height recorder, and motion-picture and electronic-flash photographic equipment. Measurements of water contacts, displacements, velocities, and accelerations were recorded on the oscillograph, along with 0.01-second timing. The wave recorder and the electronic-flash camera were correlated with the oscillograph by means of electrical pulses. Accelerations in the vertical direction were measured by oil-damped unbonded strain-gage accelerometers with frequency responses flat to 60 cycles per second.

Initial contact of the penetrating hydro-ski with the water and rebound from the water were determined from a pulse produced by an electrical circuit which was completed by the water through a contact at the stern. On the rough-water impacts forward portions of the ski frequently contacted first, and corrections were applied to the water-contact indication. Horizontal velocity was obtained from photoelectric-cell indications of horizontal displacement and from the recorded time. Vertical displacement was obtained from a slide wire, and vertical velocity was obtained from electrical differentiation of the slide-wire displacement.

Wave height was recorded with an NACA optical wave-height recorder which was mounted on the carriage so as to project a spot of light on the surface of the water just forward of the model. The spot on the water surface was recorded by a film drum located so that the rise and fall of the water surface resulted in a trace moving across the film. This wave-height recorder is described fully in reference 14. Wave length was obtained from water contacts which were spaced along the tank wall at known distances and which flashed neon-light signals to the wave-maker operator.

The photographic equipment used to observe the cavity generated by the hydro-ski and model consisted of a 16-millimeter motion-picture camera operated at 64 frames per second and a 35-millimeter stereocamera. These cameras were mounted on the underside of the testing carriage at 7 feet above the water surface and about 6 feet to the rear of the model so as to photograph the flow and the water cavity generated in the vicinity of the stern of the main model. For a few tests the stereocamera was moved to the nose of the carriage in order to obtain a front view of the impact flow. The motion of the water was stopped by an electronic flash of 20 microseconds duration. The camera and the flash were triggered by a small switch on the boom linkage which was actuated at preset

depths of immersion. The triggering signal was recorded on the oscillo-
graph for correlation purposes. In this manner a single pair of stereo-
photographs was obtained on each test. The stereophotographs obtained
were in the form of color transparencies which could be effectively
analyzed in a stereoviewer or from which prints could be made. Viewing
of stereophotographs is described in the appendix.


## ACCURACY OF DATA


In general, the data obtained are believed to be accurate to within
the following limits:

| | |
|---|---:|
| Horizontal velocity, ft/sec | ±0.5 |
| Vertical velocity, ft/sec | ±0.2 |
| Vertical displacement, ft | ±0.02 |
| Acceleration, g | ±0.2 |
| Weight, lb | ±10 |
| Time, sec | ±0.002 |
| Wave height, ft | ±0.10 |
| Wave length, ft | ±1.0 |


## TEST PROCEDURE


This investigation consisted of a series of impacts in smooth water
followed by several tests in rough water with several impacts during
each test. All impacts were made at a dropping weight of 1,375 pounds
($C_\Delta$ for model is 3.6, $C_\Delta$ for penetrating hydro-ski is 111). Through-
out each impact a lift force equal to the total weight of the model was
applied to simulate a wing lift of 1g, as described in reference 12.

The impacts in smooth water were made at trim angles of $8^\circ$, $16^\circ$,
and $30^\circ$ over a range of initial flight-path angles from $3.0^\circ$ to $19.9^\circ$.

The tests in rough water were made at a trim angle of $8^\circ$ and at
initial flight-path angles from $4.1^\circ$ to $7.4^\circ$. The last test (25) was
made with the hydro-ski removed and was made at loading conditions
which repeated those of tests 21 and 22. The weight of the removed
hydro-ski was replaced on the model to hold the weight at 1,375 pounds.
All rough-water tests were made into essentially the same wave spectrum,
the operation of the wavemaker being held constant for each of the
tests. The measured waves varied in length from 14 to 17 feet (1.4 to
1.7 model lengths) and in height from 1.2 feet to 2.00 feet. The wave
spectrum consisted of steep waves approaching breaking, breaking waves,

and milder waves subsequent to the breaking. As the model traveled through several waves during each test, data for four or five impacts were obtained for each. Since the model was not a true dynamic model, the sequence of the impacts is not representative of flight conditions. However, each impact can be considered as an independent impact representing landing conditions as designated by the sequence of the impacts.

RESULTS

The experimental data obtained in this investigation are presented in table I for each of the smooth-water impacts and in table II for each of the rough-water impacts. Table I shows the measured values of loads and motions at water contact, at maximum load factor, at maximum draft, and at exit from the water. Table II shows the measured values of load at contact with the wave and at maximum load factor and also the length, height, and slope of the waves upon which each impact was made.

Smooth-Water Loads

Figure 3 shows the variations of maximum lift coefficient with flight-path angle in smooth water for $\tau = 8^\circ$, $16^\circ$, and $30^\circ$. This figure shows that at each of the trim angles the model with the penetrating hydro-ski experiences less maximum load than the model without the penetrating hydro-ski (ref. 10). By using the curves of figure 3, the ratio of maximum lift coefficient with the hydro-ski to maximum lift coefficient without the hydro-ski was obtained for $\gamma_0 = 5.5^\circ$, $10^\circ$, and $15^\circ$. The variation of this ratio with trim angle is shown in figure 4. This variation shows that the maximum lift coefficient for the model with the hydro-ski is about 66 percent of the lift coefficient without the hydro-ski at $\tau = 30^\circ$ and $\gamma_0 = 15^\circ$. At the low trim angle of $8^\circ$ and at the low flight-path angle of $5.5^\circ$, the lift coefficient with the hydro-ski is only 34 percent of the lift coefficient without the hydro-ski. These data indicate that the installation of the penetrating hydro-ski results in reductions in maximum load of from 34 percent to 66 percent over the range of smooth-water impacts investigated.

In figure 5 the variations of maximum draft coefficient with trim and flight-path angles in smooth water are shown for the models with and without the penetrating hydro-ski. These data indicate that the installation of this hydro-ski results in approximately doubling the stroke through which the impact loads are applied to the model over the range of smooth-water impacts investigated.

Rough-Water Loads

The data of this investigation for smooth water can be considered
as establishing fundamental relationships for many rough-water loading
conditions.  In previous investigations (refs. 4, 7, and 13), it has
been shown that the impact process in rough water can be rotated by the
amount of the wave slope and treated as a smooth-water impact (by using
effective velocity and effective trim and flight-path angles).  However,
this application of the smooth-water impact is limited to impacts on
wave flanks where the wave slope is constant over a distance of the
order of the model length or greater (ref. 7).  In short choppy waves
such as those where wave length is equal to one to two model lengths,
the wave surface offers no flat plane upon which the impact of the model
can occur.  Therefore, the application of smooth-water data to this type
of impact is limited to a consideration of velocity effects, as trim
and flight-path angles relative to the curved water surface cannot be
well handled.  In the present rough-water tests the only consideration
was for impacts of this type, where the application of smooth-water data
by rotation of the axis is less accurate.

A typical profile of the waves in which the landing impacts were
made is shown in figure 6.  Although the waves were generated by the
wavemaker with a combined flapper-plunger-type motion at nearly constant
speed and amplitude, the height, length, and shape varied somewhat.  The
variations are attributed to the breaking of the crests as the waves
traveled down the tank.  Just prior to the breaking of a wave, the crest
became rather sharp in shape, but subsequent to the breaking the wave
crest became flat in shape.  From figure 6 it is seen that the slope
along the flank of the wave was constant only for very short distances
when compared with the length of the model.  With these larger variations
in wave shape relative to model length, small errors in establishing the
location of the impact along the wave resulted in poor accuracy in
defining the slope of the wave at the point contacted.  Therefore, the
wave height and length alone were used to define wave slope in the anal-
ysis of the data.  From table II it is observed that the wave slope $\theta$
is generally greater than the trim angle of the model ($8^\circ$) and, there-
fore, the range of model trim angle relative to the wave surface includes
negative trim-angle impacts.

The computed values of maximum lift coefficient $C_{L,max}$ are shown
(table II) to vary from 0.015 to 0.440.  All impacts were made at trim
angles of $8^\circ$ on wave slopes between $7^\circ$ and $16^\circ$.  Although these varia-
tions in flight-path angle and in wave size and shape result in varia-
tions in $C_{L,max}$, it is believed that the variations in $C_{L,max}$ are
largely caused by the changes in location of the impacts along the wave
profile.  Generally speaking, the first impacts of each test were mild

impacts on the crests of the waves, and the subsequent impacts were more severe and deeper down on the wave flanks.

The nature and sequence of the impacts can be better understood by considering time histories of a test. Time histories of the impact load factor, draft, and vertical velocity for one test (number 23) are shown in figure 7 to indicate the nature of the loads and motions experienced by the model with the penetrating hydro-ski. From these time histories it is seen that on first impact the hydro-ski briefly impacts through the crest of a wave. The loads encountered on this impact are too small in magnitude and in duration to affect the constant vertical velocity. Following the first impact, the hydro-ski clears the trough of the wave and enters the flank of the following wave where peak load factors of $\frac{3}{4}g$ are built up, first applied mainly on the hydro-ski and then applied on the combined hydro-ski and model. During this impact the vertical velocity is reduced from over 5 feet per second to less than 3 feet per second. Following this impact the hydro-ski remains in contact with the trough of the wave and applies a sustained load $(n_i = 1/2)$ to the model. On the third impact the load builds up to values of $n_i = 1\frac{1}{2}$, and the vertical velocity is reduced to almost zero. The draft remains essentially constant following the impact; the immersion of the hydro-ski and its load varies with the profile of the wave trough. The fourth impact takes place at near zero vertical velocity, at which time a load peak of $n_i = 1$ is reached and the model and hydro-ski are driven into an upward flight path (negative $\gamma$). The multipeak load factors during the impacts are complex, not only because of the hydro-ski arrangement but because of the generation of cavities by the hydro-ski (as discussed in the "Cavity Generation in Smooth and Rough Water" section) and because of the multipeak characteristics of the transverse shape of the model (see ref. 10). From the time history of figure 7 it is observed that the loads in rough water are applied gradually, are mild in magnitude, and are possibly alleviated by sustained loads applied by the hydro-ski as the model passes through the wave troughs.

In figure 8 the maximum lift coefficients obtained with the penetrating hydro-ski are compared with those obtained without the hydro-ski. Test number 25 was made without the hydro-ski and at landing conditions similar to those of tests 21 and 22, which were made with the hydro-ski. In figure 8 the loads for each impact of these three tests are compared. Figure 8 shows the maximum lift coefficient for each of the impacts and also the ratio of the maximum lift coefficient with the hydro-ski to the maximum lift coefficient without the hydro-ski. These data show that on the first impact the maximum lift with the hydro-ski was about 0.2 of the lift without the hydro-ski. On the second impact the lift with the hydro-ski was a little more than half of the lift without, and on the third impact the lift was nearly the same for both

cases. This comparison indicates that for the impacts where the model
without the hydro-ski experiences its most severe loads, the installa-
tion of this hydro-ski results in load reductions of the order from
50 to 80 percent.


## Cavity Generation in Smooth and Rough Water

The motion pictures obtained showed that the penetrating hydro-ski
generated flow conditions of importance from the standpoint of impact
loads. General development of the flow and growth of a cavity during
each impact were studied from the motion pictures, and detail observa-
tions of stopped motion of the water were made from electronic flash
photographs. The electronic flash photographs were obtained as stereo-
photographs in the form of color transparencies which were studied in a
viewer. These studies showed rather clear cavities cut into the water
with steep cavity walls extending as a sheet of water well above the
undisturbed water level. The width of the cavity, the separation of the
cavity walls, and the formation of light spray were found to vary with
trim and flight-path angles and with the depth of immersion.

In order to illustrate the flow conditions observed, typical pairs
of stereophotographs are presented in black and white in figures 9
to 13. Since each pair consists of nearly identical two-dimensional
photographs, either may be viewed as a conventional photograph for detail
study. In addition, all pairs of photographs are accurately mounted and
can be viewed stereoscopically in order to observe relative positions
of the model, the cavity, and the spray in space. Instructions for
stereoscopic viewing of the photographs are presented in the appendix.

In figure 9, front views of two of the 30° trim-angle impacts are
shown with the hydro-ski stern immersed 13 inches below the undisturbed
water surface. At this immersion the stern of the main model is immersed
7 inches. In figure 9(a) the hydro-ski is clearly seen with a small
amount of light spray forward of its nose. The wall of the side spray
is somewhat to the rear and is shown to impinge on the main model near
the chine. Apparently, some of this impinging spray flows inward along
the bottom of the model and is seen as light spray in the center, just
below the keel of the model. A comparison of figures 9(a) and 9(b) shows
that with the increase of horizontal velocity for the lower flight-path
angle, the light forward spray is increased and the height of the side
and rearward spray is also increased.

The cavity and cavity walls are shown more clearly in photographs
taken at the rear of the model for two impacts at a hydro-ski stern
immersion of 9 inches. (See, for example, fig. 10.) The two impacts
shown are for low flight-path angles of about 3° for trim angles of 16°
and 8°. For these trim angles and for 9-inch hydro-ski stern immersion,

the stern of the main model was above the undisturbed water surface. These photographs show that the small hydro-ski causes an impressive channel between steep cavity walls of spray. Figure 10(a) shows that the spray walls are sufficiently apart to clear the full beam of the main model (22 in.). The full beam of the model is not visible in figure 10(b); however, at the top of the photographs there are shown disturbances in the spray wall caused by the model being impinged upon by the upper portion of the spray wall. This impingement is explained by the full length of the hydro-ski being immersed and the resulting walls of spray from the narrow bow of the hydro-ski being inboard of the model chines. Photographs of complete immersion of the hydro-ski at both trim angles were obtained at higher flight-path angles.

In figures 11 and 12 impacts at three higher flight-path angles are shown. These photographs were taken at a hydro-ski stern immersion of 18 inches for $\tau = 16°$ and $\tau = 8°$. In these photographs the hydro-ski is completely below the undisturbed water level, with a hydro-ski bow immersion of 2 inches at $\tau = 16°$ and 10 inches at $\tau = 8°$. These photographs show a deep, wide cavity being cut into the water surface by the hydro-ski. The stern of the main model is down in the cavity, free of contact with solid water, and contacted only by the impingement of light spray. This ventilated portion of the model bottom is nearly flat in transverse shape and is generally responsible for a substantial buildup of load on models of this type without hydro-ski installation (see ref. 10). Therefore, it is indicated that the cavity formed by the hydro-ski is partly responsible for the reductions in load experienced by the main model. From figures 11 and 12 it is seen that the walls of the cavity or spray do impinge upon the chine regions of the model and, apparently, are directly responsible for some loading of the model. However, this type of loading has the adventage of being applied over a limited area at a time subsequent to initial buildup of the load. (See time history given in fig. 7.) The unsymmetrical appearance of the spray-wall complexities is largely attributed to the offcenter location of the lighting and camera.

Figure 13 shows photographs obtained during two impacts in rough water at 8° trim angles and initial flight-path angles of about 7°. The photographs were taken at the instants when the hydro-ski stern was about 10 inches below the level of the undisturbed water. Figure 13(a) shows the cavity left in the crest of the first wave encountered, the undisturbed trough following this wave, and the cavity developed in the second wave crest where the impact is taking place. This photograph illustrates the ability of the penetrating hydro-ski to eliminate impacts of the model with wave crests by creating a cavity through which the main step or stern can pass. Figure 13(b) illustrates an impact where the cavity and flow generation are largely hidden by the diffusion of spray. It is observed from this photograph that the wall of spray

generated with the cavity is thin and has an apparent thickness of only a fraction of an inch.

In general, the motion pictures and stereophotographs of this investigation indicate that the small hydro-ski penetrates through the water with little disturbance other than the spray and flow generated by the small braces at the bow. As the hydro-ski pierced through the water, it developed cavities and flow conditions which alleviated the load applied directly to the main model.

## GENERAL OBSERVATIONS ON THE PENETRATING HYDRO-SKI

From the result obtained, it is indicated that a small penetrating hydro-ski might be a practical device for enabling high-speed aircraft to successfully withstand rough-water landing loads. It has been shown that with a small penetrating hydro-ski, substantial reductions in impact loads were obtained. These load reductions can be attributed to the small size of the penetrating hydro-ski, to the stroke or displacement through which the hydro-ski load was the only load applied to the model, and to generation of a cavity by the small hydro-ski so as to limit contact of the model with solid water.

The effects of hydro-ski size or beam loading on impact loads have been investigated and are reasonably well established. However, effects of the location of a small hydro-ski below the main model and the effects of cavity generation by a hydro-ski appear to merit further consideration. Photographs of cavity generation by hydro-skis of other shapes have indicated cavity widths of more than five times the beam of the hydro-ski. From studies of effects of hydro-ski shape and velocity on cavity sizes, it might be established that cavities of the size reported in the present investigation might be more efficiently generated by much smaller penetrating hydro-skis suitable for very high-speed aircraft.

There are indications that the full value of the penetrating hydro-ski can be realized only by considering the hydro-ski as a device for smoothing out the irregularities of the rough seaway. The penetrating hydro-ski must, therefore, pierce through waves, open cavities in wave crests, and maintain contact with the wave surface through the trough so that a nearly constant load is applied to the model irrespective of the wave contour.

CONCLUSIONS

An experimental investigation of impact loads obtained with a small penetrating hydro-ski mounted below a larger model resulted in the following conclusions:

1. Installation of this penetrating hydro-ski results in reductions in maximum load of from 34 to 66 percent over the range of smooth-water impact conditions investigated.

2. Installation of this penetrating hydro-ski approximately doubles the stroke (vertical displacement) through which the impact loads are applied to the model for the range of smooth-water conditions investigated.

3. With this penetrating hydro-ski installed, the impact loads in rough water are gradually applied and are mild in magnitude.

4. For rough-water impacts where the model without the penetrating hydro-ski experiences its most severe loads, the installation of this penetrating hydro-ski results in load reductions of from 50 to 80 percent.

5. Photographic studies of the flow and cavity generation of this penetrating hydro-ski indicate that the penetrating hydro-ski moved smoothly through the water, opened impressive cavities in the surface of the water, and alleviated the load applied directly to the main model.


Langley Research Center,
        National Aeronautics and Space Administration,
                Langley Field, Va., October 1, 1958.

APPENDIX


NOTES ON VIEWING STEREOPHOTOGRAPHS


Stereophotographs taken with lenses separated by the normal inter-ocular distance are basically the views normally seen by each individual eye. For stereoviewing, the pair of photographs must lie in a flat plane, and the two eyes must be coplanar with the corresponding points in the two photographs; that is, similar cr corresponding points in the pair of stereophotographs must lie accurately in the same plane as the two eyes. The plane of the paper should te approximately perpendicular to the line of sight. A very slight angle of roll with respect to the eyes will prevent the viewer from seeing a three-dimensional picture.

The following are suggested steps of procedure which may help in viewing stereophotographs in three dimensions:

1. Hold the page flat, in good light, and at a comfortable reading distance.

2. Hold the page squarely so that each of the pair of stereophoto-graphs is at the same distance from the eyes and so that each photo-graph is level. Corresponding points in the photographs should lie in a flat plane with the eyes.

3. If glasses are normally worn for reading, use them in viewing the stereophotographs.

4. As an aid to seeing the left picture with the left eye and the right picture with the right eye, place a piece of cardboard of about a foot square perpendicular to the picture with the edge along the dividing line between the photographs.

5. Another aid in stereoviewing is the use of an inexpensive pair of strong magnifying spectacles which permit viewing of the magnified pictures at very close range. Mask the inner portion (about one-fourth) of each lense at the nose to block crossviewing of the pictures.

6. The viewing distances between the eyes and the picture should be varied gradually until three-dimensional viewing is obtained. If mag-nifying spectacles are used, they should be moved gradually away from the eyes until the optimum position for stereoviewing is found.

The viewing of stereophotographs is thoroughly discussed in refer-ence 15, and the underlying principles of steroscopy are found in reference 16.

REFERENCES

1. Edge, Philip M., Jr.: Hydrodynamic Impact Loads in Smooth Water for a Prismatic Float Having an Angle of Dead Rise of $10°$. NACA TN 3608, 1956.

2. McArver, A. Ethelda: Water-Landing Investigation of a Model Having Heavy Beam Loadings and $0°$ Angle of Dead Rise. NACA TN 2330, 1951.

3. Batterson, Sidney A., and McArver, A. Ethelda: Water Landing Investigation of a Model Having a Heavy Beam Loading and a $30°$ Angle of Dead Rise. NACA TN 2015, 1950.

4. Edge, Philip M., Jr.: Impact-Loads Investigation of Chine-Immersed Models Having Concave-Convex Transverse Shape and Straight or Curved Keel Lines. NACA TN 3940, 1957.

5. Edge, Philip M., Jr.: Impact-Loads Investigation of Chine-Immersed Model Having a Circular-Arc Transverse Shape. NACA TN 4103, 1957.

6. Edge, Philip M., Jr., and Mixson, John S.: Impact-Loads Investigation of a Chine-Immersed Model Having a Longitudinally Curved Bow and a V-Bottom With a Dead-Rise Angle of $30°$. NACA TN 4106, 1957.

7. Markey, Melvin F., and Carpini, Thomas D.: Rough Water Impact-Load Investigation of a Chine-Immersed V-Bottom Model Having a Dead-Rise Angle of $10°$. NACA TN 4123, 1957.

8. Edge, Philip M., Jr.: Hydrodynamic Impact Loads of a $-20°$ Dead-Rise Inverted-V Model and Comparisons With Loads of a Flat-Bottom Model. NACA TN 4339, 1958.

9. Miller, Robert W.: Water-Landing Investigation of a Flat-Bottom V-Step Model and Comparison With a Theory Incorporating Planing Data. NACA TN 2932, 1953.

10. Edge, Philip M., Jr., and Mason, Jean P.: Hydrodynamic Impact Loads on $30°$ and $60°$ V-Step Plan-Form Models With and Without Dead Rise. NACA TN 4401, 1958.

11. Mixson, John S.: The Effect of Beam Loading on Water Impact Loads and Motions. NASA MEMO 1-5-59L, 1959.

12. Batterson, Sidney A.: The NACA Impact Basin and Water Landing Tests of a Float Model at Various Velocities and Weights. NACA Rep. 795, 1944. (Supersedes NACA WR L-163.)

13. Miller, Robert W.: Hydrodynamic Impact Loads in Rough Water for a Prismatic Float Having an Angle of Dead Rise of 30°. NACA TN 1776, 1948.

14. Edge, Philip M., Jr.: Instrumentation for Investigation of Seaplane Impact Loads in Waves. Proc. First Conf. on Coastal Eng. Instruments (Berkeley, Calif., Oct. 31 - Nov. 2, 1955), Council on Wave Res., The Eng. Foundation, 1956, pp. 213-226.

15. Morgan, Willard D., and Lester, Henry M.: Stereo Realist Manual. Morgan & Lester (New York), c.1954.

16. McKay, Herbert C.: Three-Dimensional Photography. Principles of Stereoscopy. American Photography Book Dept. (New York), c.1953.

TABLE I.- SMOOTH-WATER DATA

| Test no. | Trim, $\tau$, deg | At contact $\dot{z}_o$, ft/sec | At contact $\dot{x}_o$, ft/sec | At contact $\gamma_o$, deg | At $n_{i,max}$ t, sec | At $n_{i,max}$ $n_i$ | At $n_{i,max}$ z, ft | At $n_{i,max}$ $\dot{z}$, ft/sec | At $n_{i,max}$ $C_L$ | At $z_{max}$ t, sec | At $z_{max}$ $n_i$ | At $z_{max}$ z, ft | At exit t, sec | At exit $\dot{z}$, ft/sec |
|---|---|---|---|---|---|---|---|---|---|---|---|---|---|---|
| 1 | 8 | 4.1 | 75.8 | 3.08 | 0.139 | 0.57 | 0.53 | 6.5 | 0.04 | 0.425 | 0.24 | 0.91 | --- | --- |
| 2 |  | 4.9 | 65.4 | 4.29 | .109 | .54 | .51 | 7.8 | .05 | .539 | .24 | 1.31 | --- | --- |
| 3 |  | 4.8 | 40.4 | 6.82 | .493 | .28 | 1.69 | 7.7 | .07 | .675 | .18 | 1.81 | --- | --- |
| 4 |  | 8.1 | 41.2 | 11.13 | .270 | .82 | 1.77 | 12.9 | .20 | .455 | .33 | 2.09 | --- | --- |
| 5 |  | 9.5 | 36.4 | 14.67 | .244 | 1.07 | 1.94 | 15.1 | .32 | .440 | .41 | 2.36 | --- | --- |
| 6 |  | 9.4 | 26.0 | 19.87 | .273 | .93 | 1.17 | 15.0 | .51 | .566 | .19 | 2.27 | --- | --- |
| 7 | 16 | 3.9 | 71.4 | 3.13 | 0.201 | 0.65 | 0.66 | 2.1 | 0.05 | 0.336 | 0.46 | 0.76 | 0.803 | -1.5 |
| 8 |  | 4.0 | 65.4 | 3.48 | .228 | .56 | .73 | 2.0 | .06 | .358 | .39 | .83 | 1.018 | -.7 |
| 9 |  | 4.0 | 49.3 | 4.60 | .310 | .39 | .98 | 1.8 | .07 | .460 | .26 | 1.07 | --- | --- |
| 10 |  | 5.6 | 44.8 | 7.08 | .358 | .56 | 1.43 | 1.4 | .12 | .418 | .55 | 1.46 | --- | --- |
| 11 |  | 8.0 | 41.0 | 11.01 | .296 | .95 | 1.68 | 3.1 | .23 | .386 | .74 | 1.91 | --- | --- |
| 12 |  | 9.4 | 37.0 | 14.28 | .286 | 1.13 | 1.35 | 3.9 | .33 | .386 | .75 | 2.23 | --- | --- |
| 13 |  | 9.4 | 26.7 | 19.43 | .309 | .96 | 1.07 | 4.8 | .50 | .474 | .47 | 2.67 | --- | --- |
| 14 | 30 | 3.8 | 71.4 | 3.03 | 0.270 | 0.83 | 0.79 | 1.1 | 0.07 | 0.310 | 0.76 | 0.80 | 0.768 | -1.5 |
| 15 |  | 4.7 | 59.9 | 4.50 | .249 | .76 | .97 | 2.1 | .09 | .339 | .51 | 1.05 | .984 | -.5 |
| 16 |  | 5.6 | 44.6 | 7.11 | .220 | .58 | 1.10 | 3.9 | .12 | .435 | .41 | 1.47 | --- | --- |
| 17 |  | 9.2 | 49.0 | 10.67 | .307 | 1.18 | 1.62 | 1.6 | .20 | .332 | 1.18 | 1.90 | .774 | -4.9 |
| 18 |  | 9.4 | 41.7 | 12.65 | .355 | 1.07 | 1.41 | 1.5 | .25 | .385 | 1.00 | 2.15 | .885 | -4.6 |
| 19 |  | 9.4 | 32.3 | 16.20 | .395 | 1.02 | .99 | 2.0 | .38 | .440 | .94 | 2.56 | 1.076 | -3.8 |

TABLE II.- ROUGH-WATER DATA

$$(\tau = 8°)$$

| Test no. | Impact no. | At contact | | | | At $n_{i,max}$ | | | Wave conditions | | |
|---|---|---|---|---|---|---|---|---|---|---|---|
| | | $t,$ sec | $\dot{z},$ ft/sec | $\dot{x},$ ft/sec | $\gamma,$ deg | $t,$ sec | $n_i$ | $C_{L,max}$ | $l,$ ft | $h,$ ft | $\theta,$ deg |
| With penetrating hydro-ski | | | | | | | | | | | |
| 20 | 1 | 0 | 5.1 | 70.6 | 4.12 | 0.007 | 0.18 | 0.015 | 17.1 | 1.42 | 9.43 |
| | 2 | .120 | 5.0 | 69.7 | 4.12 | .133 | 1.56 | .135 | 16.5 | 1.15 | 7.94 |
| | 3 | .258 | 3.7 | 68.6 | 3.12 | .274 | 1.74 | .155 | 14.7 | 1.35 | 10.41 |
| | 4 | .490 | .0 | 69.2 | .02 | .537 | 1.05 | .092 | 15.0 | 1.30 | 9.83 |
| 21 | 1 | 0 | 5.1 | 59.1 | 4.90 | 0.007 | 0.22 | 0.026 | 16.3 | 1.76 | 12.19 |
| | 2 | .158 | 5.1 | 58.3 | 5.04 | .175 | 1.05 | .129 | 16.8 | 1.68 | 11.31 |
| | 3 | .335 | 3.8 | 58.3 | 3.68 | .452 | 1.43 | .178 | 15.9 | 1.55 | 11.03 |
| | 4 | .639 | -.3 | 57.1 | -.28 | .670 | .80 | .104 | 14.4 | 1.58 | 12.38 |
| 22 | 1 | 0 | 5.1 | 58.8 | 4.96 | 0.038 | 0.41 | 0.050 | 15.5 | 1.32 | 9.67 |
| | 2 | .240 | 4.8 | 58.3 | 4.70 | .253 | 1.26 | .155 | 17.4 | 1.95 | 12.63 |
| | 3 | .454 | 1.9 | 57.9 | 1.90 | .479 | 1.48 | .187 | 17.4 | 1.45 | 9.46 |
| | 4 | .717 | -.5 | 56.8 | -.53 | .763 | .61 | .080 | 14.4 | 1.77 | 13.81 |
| 23 | 1 | 0 | 5.3 | 40.8 | 7.33 | 0.007 | 0.24 | 0.056 | 16.0 | 1.05 | 7.48 |
| | 2 | .174 | 5.3 | 40.5 | 7.41 | .198 | .88 | .210 | 13.7 | 1.90 | 15.50 |
| | 3 | .453 | 2.6 | 39.1 | 3.82 | .493 | 1.71 | .440 | 14.0 | 1.73 | 13.88 |
| | 4 | .791 | .0 | 39.0 | .03 | .815 | 1.12 | .291 | 15.6 | 1.45 | 10.53 |
| 24 | 1 | 0 | 5.4 | 41.3 | 7.41 | 0.011 | 0.71 | 0.173 | | | |
| | 2 | .301 | 3.3 | 40.6 | 4.63 | .349 | .92 | .234 | | | |
| | 3 | .551 | 1.2 | 40.5 | 1.75 | .571 | 1.35 | .347 | | | |
| | 4 | .851 | -.0 | 39.2 | -.04 | .895 | 1.01 | .279 | | | |
| | 5 | 1.211 | -.4 | 38.5 | -.61 | 1.244 | .68 | .193 | | | |
| Without penetrating hydro-ski | | | | | | | | | | | |
| 25 | 1 | 0 | 5.2 | 58.3 | 5.07 | 0.008 | 1.62 | 0.199 | | | |
| | 2 | .116 | 4.4 | 57.5 | 4.34 | .150 | 1.98 | .252 | | | |
| | 3 | .340 | .2 | 57.1 | .24 | .380 | 1.49 | .192 | | | |
| | 4 | .555 | -1.1 | 56.2 | -1.15 | .603 | .83 | .111 | | | |
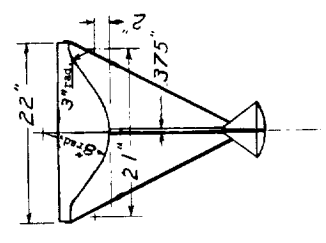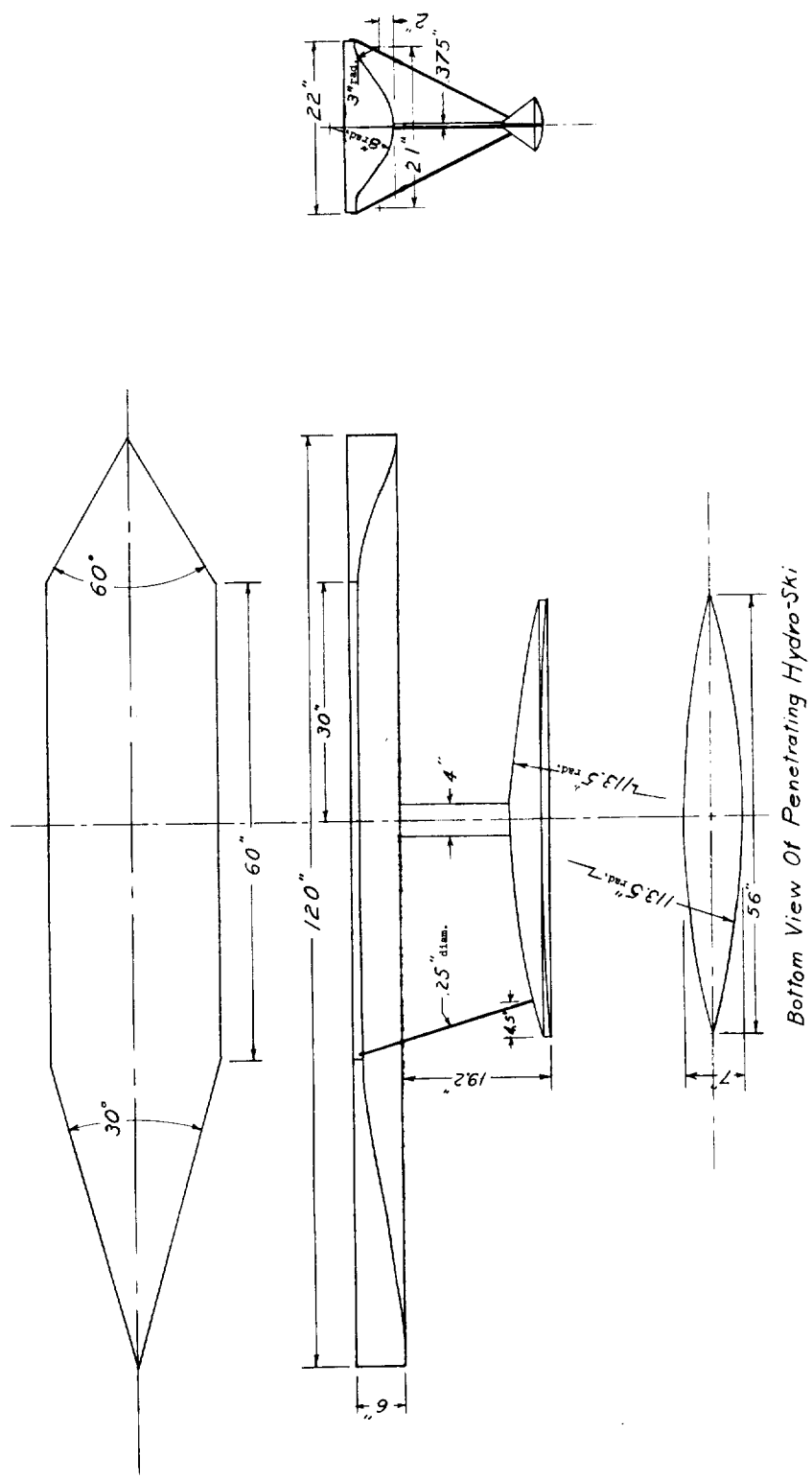
Figure 1.- Sketch of model and penetrating hydro-ski.

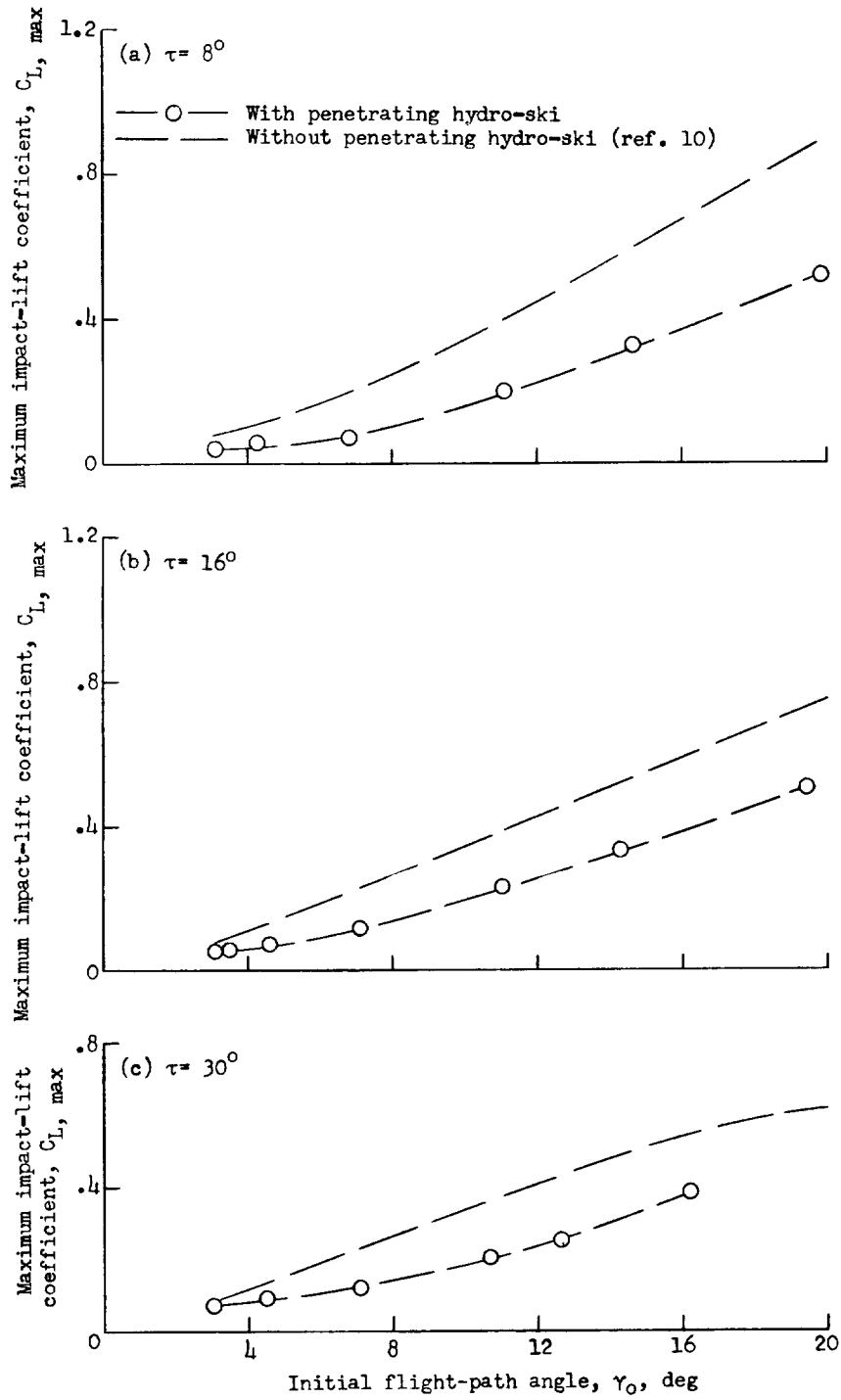Figure 2.- Model and penetrating hydro-ski mounted on carriage.    L-58-379

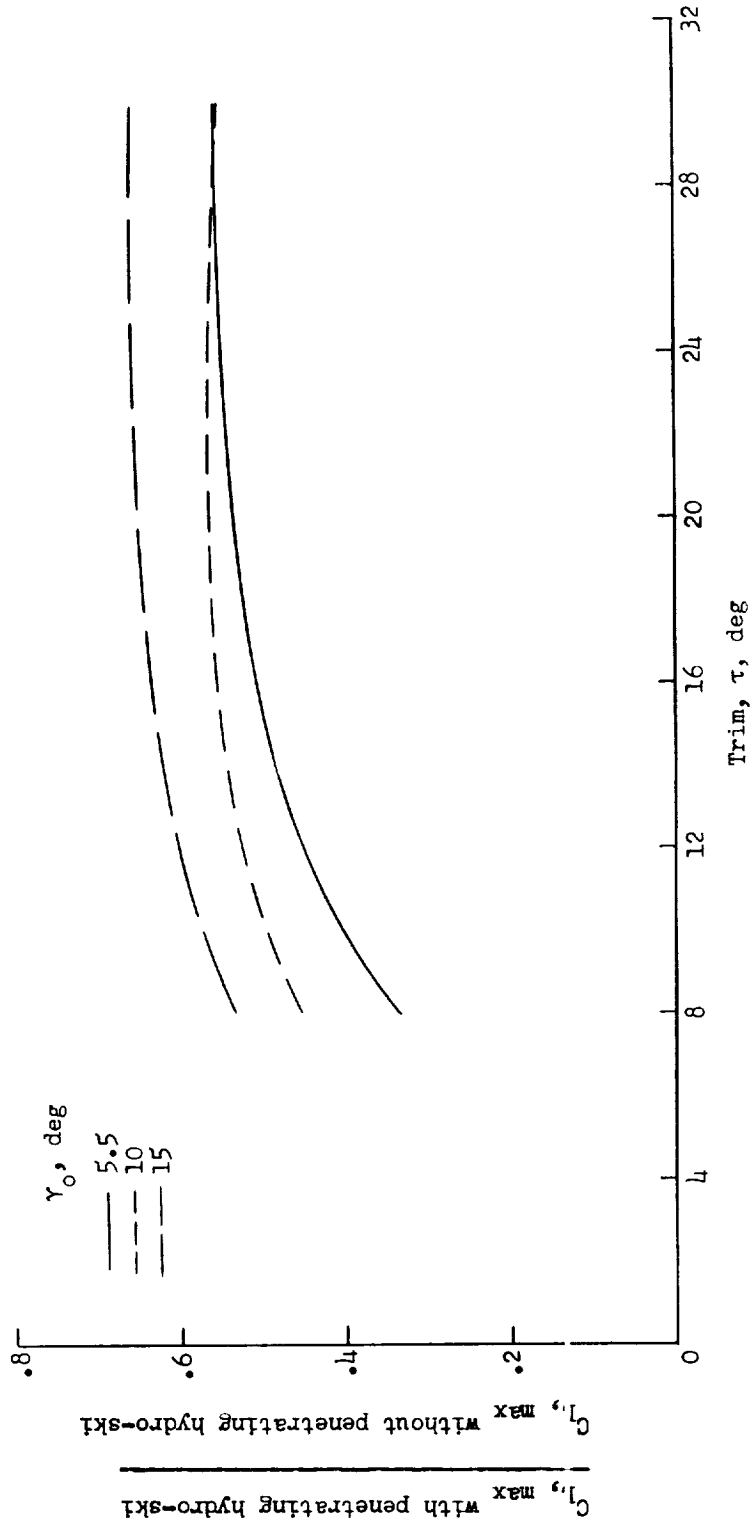Figure 3.- Variations of maximum impact-lift coefficient with initial flight-path angle in smooth water.

Figure 4.- Comparisons of maximum impact-lift coefficient for model with penetrating hydro-ski with maximum lift coefficient for model without penetrating hydro-ski in smooth water.
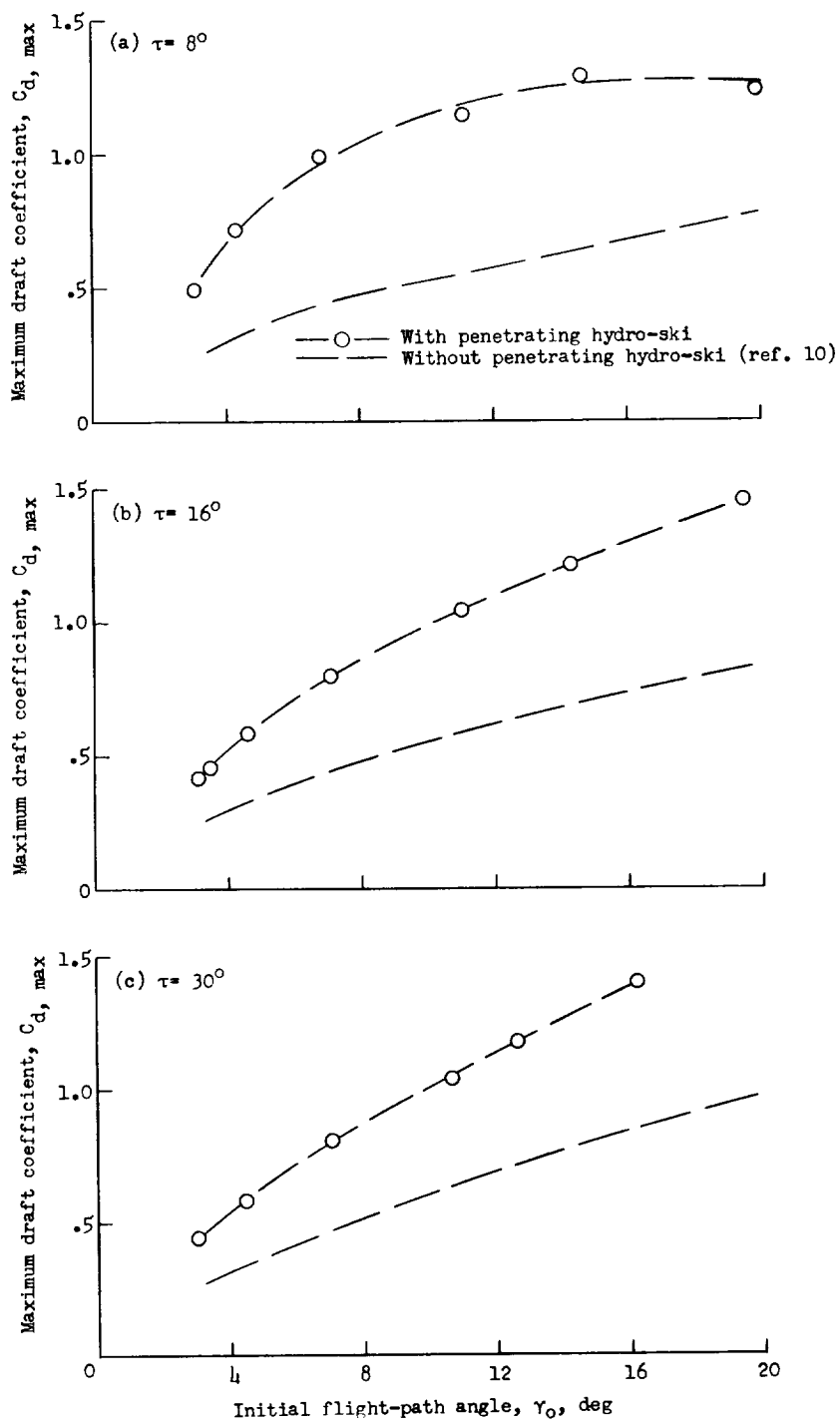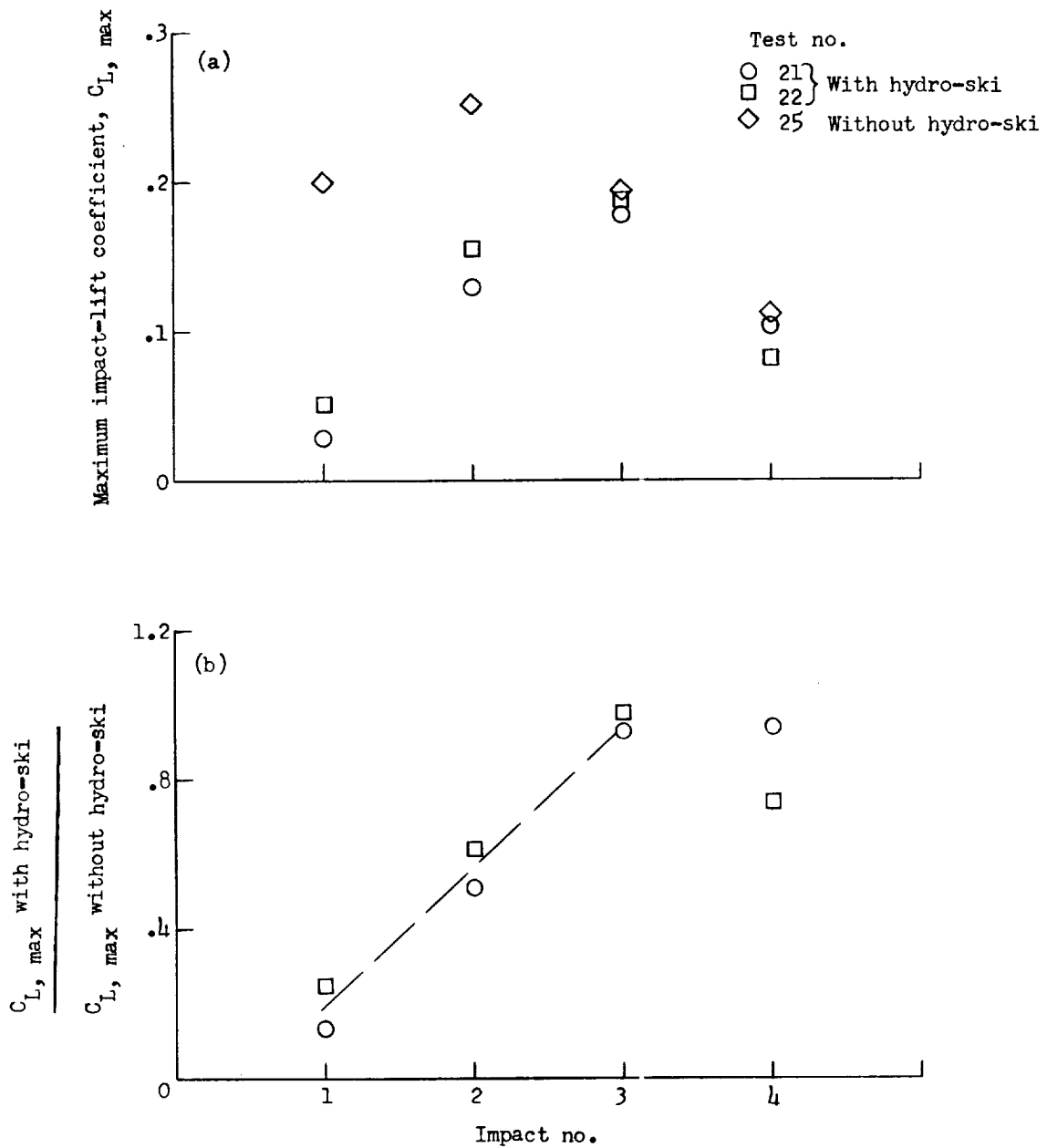
Figure 5.- Variations of maximum draft coefficient with initial flight-path angle in smooth water.
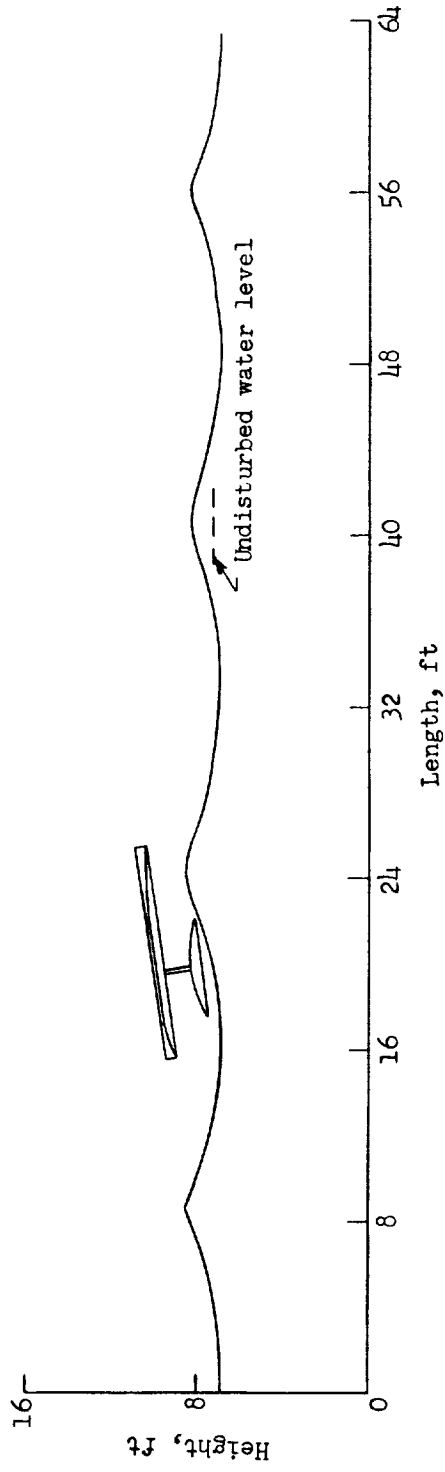
Figure 6.- Typical wave profile.  Test number 21.
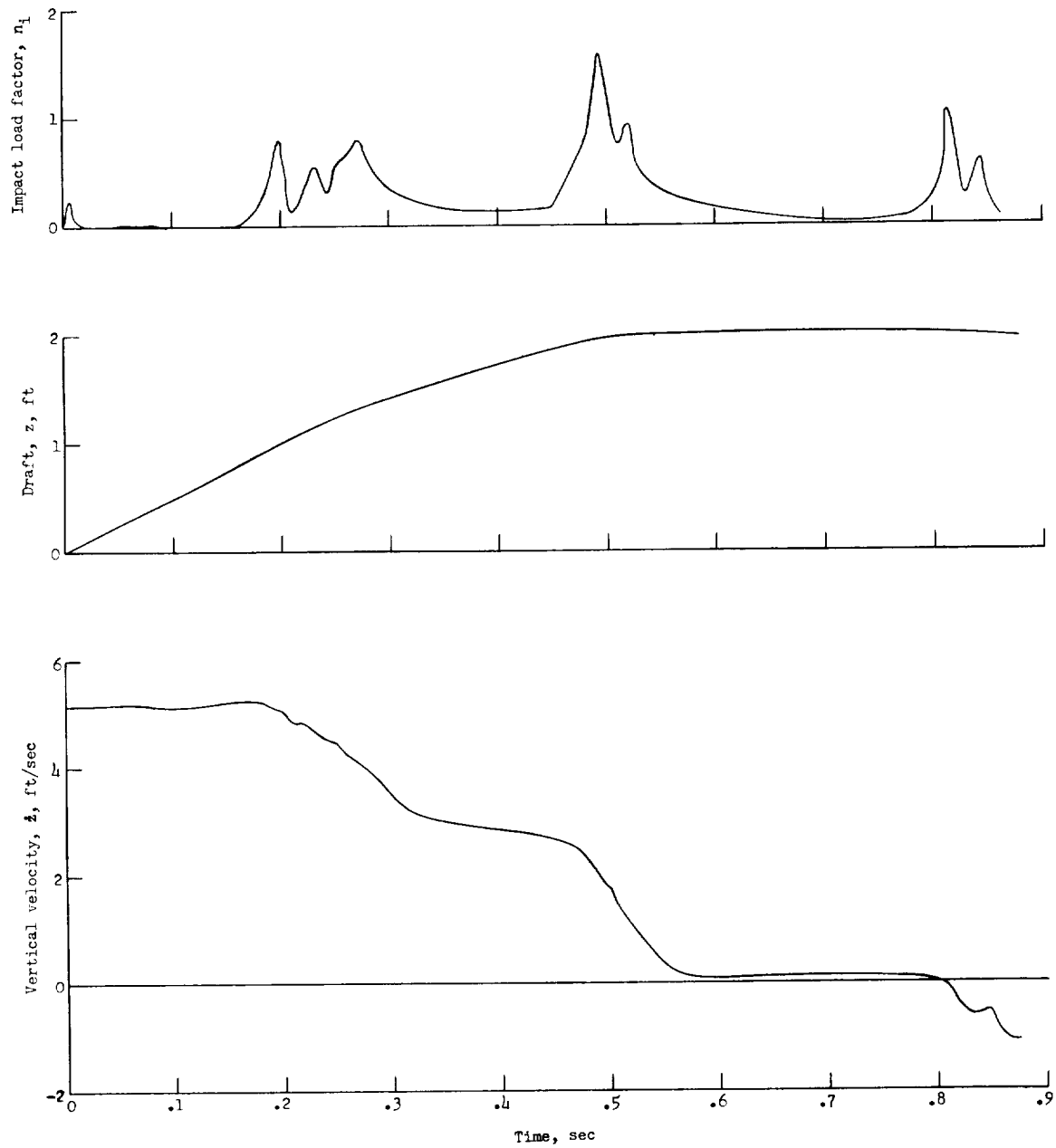
Figure 7.- Typical time histories of impact load factor, draft, and
vertical velocity of the model with the penetrating hydro-ski in
rough water. Test number 23.

Figure 8.- Comparisons of maximum impact-lif; coefficient for model with penetrating hydro-ski with maximum lift coefficient for model without penetrating hydro-ski in rough water.
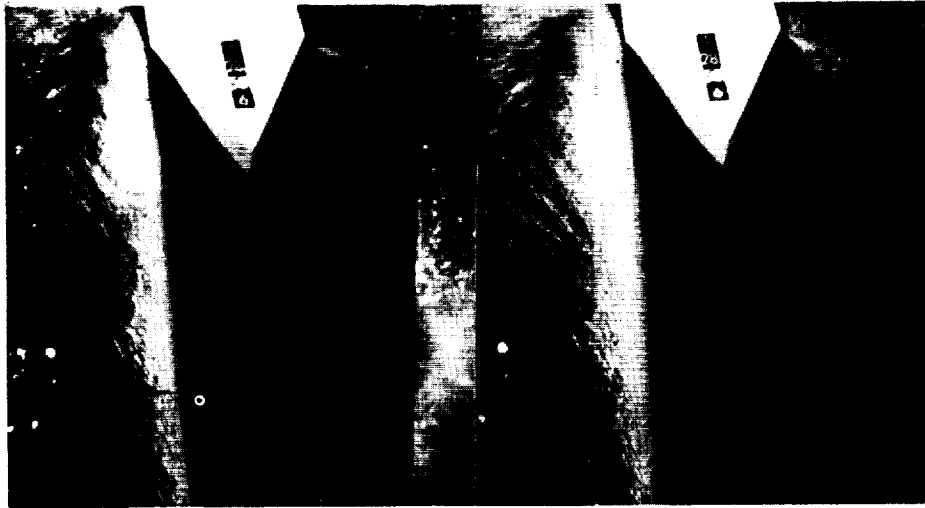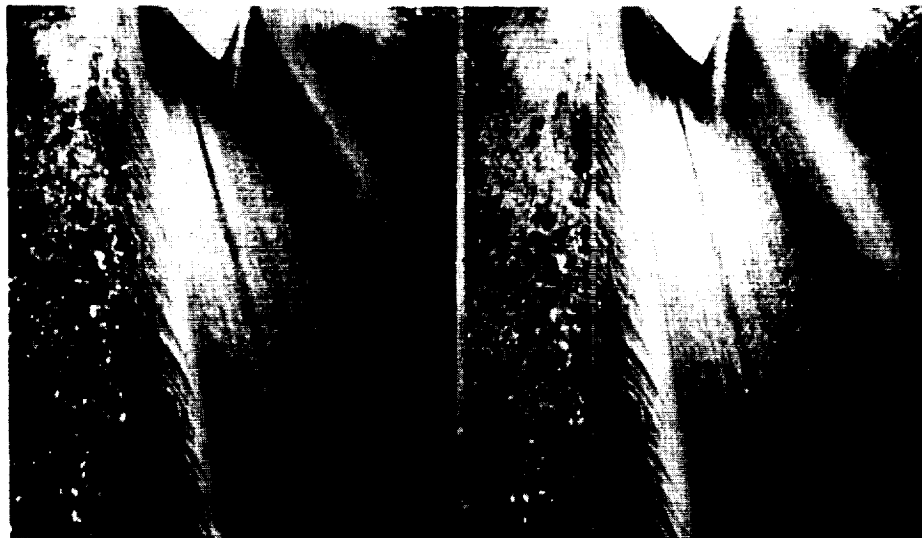
(a) $\gamma_o = 16.20^o$; $\dot{x}_o = 32.3$ fps.



(b) $\gamma_o = 10.67^o$; $\dot{x}_o = 49.0$ fps.          L-58-2553

Figure 9.- Stereophotographs of smooth-water impact of model with pene-
trating hydro-ski. Front view. Immersion of hydro-ski stern,
13 inches; $\tau = 30^o$.

28



(a)   $\tau = 16°$; $\gamma_O = 3.48°$; $\dot{x}_O = 65.4$ fps.



(b)   $\tau = 8°$; $\gamma_O = 3.08°$; $\dot{x}_O = 75.8$ fps.     L-58-2554

Figure 10.- Stereophotographs of smooth-water impact of model with pene-
    trating hydro-ski.  Rear view.  Immersion of hydro-ski stern,
    9 inches.

(a)  $\gamma_o = 11.01^\circ$; $\dot{x}_o = 41.0$ fps.



(b)  $\gamma_o = 14.28^\circ$; $\dot{x}_o = 37.0$ fps.



(c)  $\gamma_o = 19.43^\circ$; $\dot{x}_o = 26.7$ fps.          L-58-2555

Figure 11.- Stereophotographs of smooth-water impact of model with pene-
   trating hydro-ski.  Rear view.  Immersion of hydro-ski stern,
   18 inches; $\tau = 16^\circ$.

(a) $\gamma_O = 11.13^\circ$; $\dot{x}_O = 41.2$ fps.



(b) $\gamma_O = 14.67^\circ$; $\dot{x}_O = 36.4$ fps.



(c) $\gamma_O = 19.87^\circ$; $\dot{x}_O = 26.7$ fps.          L-58-2556

Figure 12.- Stereophotographs of smooth-water impact of model with pene-
trating hydro-ski.  Rear view.  Immersion of hydro-ski stern,
18 inches; $\tau = 8^\circ$.

(a) $\gamma_o = 7.33^o$; $\dot{x}_o = 40.8$ fps.

(b) $\gamma_o = 7.41^o$; $\dot{x}_o = 41.3$ fps. L-58-2557

Figure 13.- Stereophotographs of rough-water impacts of model with pene-
   trating hydro-ski. Rear view. Immersion of hydro-ski stern,
   10 inches below undisturbed water level; $\tau = 8^o$.